ARL-RP-0575 ● AUG 2016

US Army Research Laboratory

The Quasi-Static and Dynamic Response of Fine-Grained Mg Alloy AMX602: An Experimental and Computational Study

by Christopher S Meredith, Jeffrey T Lloyd, and Tomoko Sano

A reprint from Materials Science and Engineering A. 2016;673:73–82.

NOTICES

Disclaimers

The findings in this report are not to be construed as an official Department of the Army position unless so designated by other authorized documents.

Citation of manufacturer's or trade names does not constitute an official endorsement or approval of the use thereof.

Destroy this report when it is no longer needed. Do not return it to the originator.

ARL-RP-0575 ● AUG 2016

US Army Research Laboratory

The Quasi-Static and Dynamic Response of Fine-Grained Mg Alloy AMX602: An Experimental and Computational Study

by Christopher S Meredith, Jeffrey T Lloyd, and Tomoko Sano
Weapons and Materials Research Directorate, ARL

A reprint from Materials Science and Engineering A. 2016;673:73–82.

REPORT DOCUMENTATION PAGE

Form Approved
OMB No. 0704-0188

1. REPORT DATE *(DD-MM-YYYY)*	2. REPORT TYPE	3. DATES COVERED (From - To)
August 2016	Reprint	January 2015–May 2016

4. TITLE AND SUBTITLE
The Quasi-Static and Dynamic Response of Fine-Grained Mg Alloy AMX602: An Experimental and Computational Study

5a. CONTRACT NUMBER

5b. GRANT NUMBER

5c. PROGRAM ELEMENT NUMBER

6. AUTHOR(S)
Christopher S Meredith, Jeffrey T Lloyd, and Tomoko Sano

5d. PROJECT NUMBER

5e. TASK NUMBER

5f. WORK UNIT NUMBER

7. PERFORMING ORGANIZATION NAME(S) AND ADDRESS(ES)
US Army Research Laboratory
ATTN: RDRL-WMP-C
Aberdeen Proving Ground, MD 21005-5069

8. PERFORMING ORGANIZATION REPORT NUMBER
ARL-RP-0575

9. SPONSORING/MONITORING AGENCY NAME(S) AND ADDRESS(ES)

10. SPONSOR/MONITOR'S ACRONYM(S)

11. SPONSOR/MONITOR'S REPORT NUMBER(S)

12. DISTRIBUTION/AVAILABILITY STATEMENT
Approved for public release; distribution is unlimited.

13. SUPPLEMENTARY NOTES
A reprint from Materials, Science, and Engineering A. 2016;673:73–82.

14. ABSTRACT
A high strength magnesium alloy, AMX602(Mg-6%Al-0.5%Mn-2%Ca),was manufactured by the spinning water atomization process (SWAP) and extruded into bar and plate geometries. Microstructural analysis using electron backscatter diffraction revealed that the processing produces an alloy with grains between 0.5 and 5 mm, with comparatively weak texture for Mg. The plate and bar had different textures—the former had a conventional hexagonal-close-packed (HCP) rolling texture and the latter a HCP extrusion texture. Quasi-static and dynamic compression experiments were performed to probe the material's mechanical behavior in the three processing directions. The experiments on each geometry revealed different anisotropic properties induced by a change in the active deformation mechanisms. The anisotropy was more pronounced at dynamic strain rates than quasi-static. A reduced-order crystal plasticity model that demarcates twinning, basal slip, and non-basal slip mechanisms was fit to the experimental data from the plate and bar. The model was consistent with experimental data and revealed that in the plate twinning dominated yielding in the extrusion and transverse directions, but slip dominated the normal direction. Yielding in the bar was dominated by twinning in the extrusion direction, but both slip and twinning were significant in the other two directions. The model showed the different anisotropic responses were due to the different textures produced during the processing of each geometry. Lastly, our data provided the basis for considering twinning to be rate insensitive in the model, which we confirm to be valid to at least 5000 s^{-1}.

15. SUBJECT TERMS
AMX602, twinning, crystal plasticity modeling, dynamic strain rates, anisotropy

16. SECURITY CLASSIFICATION OF:			17. LIMITATION OF ABSTRACT	18. NUMBER OF PAGES	19a. NAME OF RESPONSIBLE PERSON
a. REPORT	b. ABSTRACT	c. THIS PAGE			Christopher S Meredith
Unclassified	Unclassified	Unclassified	UU	16	19b. TELEPHONE NUMBER (Include area code) 410-278-6715

Materials Science & Engineering A 673 (2016) 73–82

Contents lists available at ScienceDirect

Materials Science & Engineering A

journal homepage: www.elsevier.com/locate/msea

The quasi-static and dynamic response of fine-grained Mg alloy AMX602: An experimental and computational study

Christopher S. Meredith [a,*], Jeffrey T. Lloyd [a], Tomoko Sano [b]

[a] Army Research Lab, Impact Physics Branch, Aberdeen Proving Ground, MD, USA
[b] Army Research Lab, Lightweight & Specialty Metals Branch, Aberdeen Proving Ground, MD, USA

ARTICLE INFO

Article history:
Received 26 May 2016
Received in revised form
7 July 2016
Accepted 9 July 2016
Available online 10 July 2016

Keywords:
Magnesium alloy AMX602
Spinning water atomization process (SWAP)
Grain refinement
Anisotropy
Twinning
Crystal plasticity

ABSTRACT

A high strength magnesium alloy, AMX602 (Mg-6%Al-0.5%Mn-2%Ca), was manufactured by the spinning water atomization process (SWAP) and extruded into bar and plate geometries. Microstructural analysis using electron backscatter diffraction revealed that the processing produces an alloy with grains between 0.5 and 5 μm, with comparatively weak texture for Mg. The plate and bar had different textures–the former had a conventional hexagonal-close-packed (HCP) rolling texture and the latter a HCP extrusion texture. Quasi-static and dynamic compression experiments were performed to probe the material's mechanical behavior in the three processing directions. The experiments on each geometry revealed different anisotropic properties induced by a change in the active deformation mechanisms. The anisotropy was more pronounced at dynamic strain rates than quasi-static. A reduced-order crystal plasticity model that demarcates twinning, basal slip, and non-basal slip mechanisms was fit to the experimental data from the plate and bar. The model was consistent with experimental data and revealed that in the plate twinning dominated yielding in the extrusion and transverse directions, but slip dominated the normal direction. Yielding in the bar was dominated by twinning in the extrusion direction, but both slip and twinning were significant in the other two directions. The model showed the different anisotropic responses were due to the different textures produced during the processing of each geometry. Lastly, our data provided the basis for considering twinning to be rate insensitive in the model, which we confirm to be valid to at least 5000 s^{-1}.

Published by Elsevier B.V.

1. Introduction

Magnesium is the lightest structural metal with a specific strength similar to or exceeding that of aluminum and titanium [1]. However, commercial magnesium alloys have limited ductility, anisotropic mechanical behavior, and relatively poor corrosion resistance. The strength and ductility can be optimized through alloy development, texture modification, grain refinement, or combinations thereof [2,3]. For example, recent Mg alloy developments have consisted of enhancing precipitate hardening via microalloying by adding trace amounts of certain elements to create finely dispersed precipitates [4]. In addition, alloys with a more random texture have shown increased ductility than typically textured wrought alloys because the random texture increases the strain hardening rate, which promotes stable plastic deformation [5–7]. Furthermore, reducing the grain size increases the strength of a metal through the Hall-Petch relationship. Twinning also follows this relationship [8], but the critical stress to activate twinning increases faster than for slip as the grain size decreases, resulting in twinning being suppressed below a critical value [8,9]. Typical processing methods, e.g. rolling and extrusion, limit the ability to reduce the grain size due to Mg's limited ductility, and these methods produce sharp textures associated with increasing mechanical anisotropy, tension/compression asymmetry, and limited ductility.

Severe plastic deformation processing methods are effective at refining grain size, but they also produce sharp textures [10–13]. Equal channel angular pressing (ECAP) is able to reduce the grain size and tailor the texture for property improvement. Several authors [14–16] have performed ECAP on AZ31B which showed increased strength and reduced anisotropy while preserving ductility using specific processing routes and temperatures. The resulting basal texture is generally stronger than before, and is rotated with respect to a principal processing direction. Therefore, when determining the subsequent strength and ductility, the loading directions were at an angle with respect to the basal texture. When conventional rolled AZ31B is loaded along the

* Corresponding author.
E-mail address: christopher.s.meredith3.civ@mail.mil (C.S. Meredith).

http://dx.doi.org/10.1016/j.msea.2016.07.035
0921-5093/Published by Elsevier B.V.

processing directions, the loading direction coincides with the principal texture components, maximizing the measured the anisotropic response. The reduced anisotropic behavior and negligible change in ductility of ECAPed AZ31B is partially a consequence of the chosen loading directions, and not an intrinsic material property. When samples are cut along principle material directions, the measured yield strength differences in different directions can still vary by a factor of 2 or more, and limited ductility is observed for particular loading conditions [14,15]. In applications with complex loading conditions, where the full anisotropic material response is probed, it is unclear whether this ECAPed AZ31B will exhibit its measured strength and ductility improvement.

Rapid solidification is another technique for concurrent grain refinement and texture modification. Several authors [17–20] have used rapid solidification processes to prepare metal powders such as Fe, Mg, Al and Cu and their alloys. Additionally, the Spinning Water Atomization Process (SWAP) is capable of producing metal powders with a fine-grained microstructure [21–24]. Recently, SWAP was applied to Mg alloys and it has shown promise in producing relatively large volumes with a fine-grained microstructure and a comparatively weak texture [25–28]. SWAP consists of rapidly cooling molten material with water, which produces a coarse powder. The powder is consolidated and extruded to its bulk shape. Two candidate high strength Mg alloys, AMX602 (Mg-6%Al-0.5%Mn-2%Ca) and ZAXE1711 (Mg-1%Zn-7%Al-1%Ca-1% La), have exhibited improved ballistic performance compared with conventionally processed AZ31B [29].

An initial batch of AMX602 specimens was produced in extruded bars with a width-to-thickness ratio of 1.5:1. These specimens had reduced peak texture (compared to conventionally rolled Mg alloys), measured yield strengths of approximately 250–350 MPa, and strain-to-failures of about 10–20%, depending on the loading direction, strain rate, and sense (tension or compression) [26,27,30]. Because commercial applications need plate-like specimens with larger width-to-thickness ratios, a subsequent batch was produced with a ratio of 6:1.

In this study AMX602 was prepared by SWAP and the coarse powder was consolidated and extruded into a bar or plate with a width-to-thickness ratio of 1.5:1 and 6:1, respectively. We examined the microstructure of the plate using electron backscatter diffraction (EBSD). We performed experiments in both geometries to determine the material's mechanical behavior in compression at quasi-static and dynamic strain rates in each of the three processing directions–extrusion (ED), transverse (TD) and normal (ND) directions. Additionally, a recently developed HCP crystal plasticity model [31] was used to analyze the material's response subjected to the aforementioned loading conditions. The model was used to show that differences in the mechanical response and anisotropy of the bar and plate can be attributed to the variations in the texture between the geometries. We also show experimentally that twinning is strain rate insensitive over the wide range of strain rates tested here, up to 5000 s^{-1}, which is an assumption of the model.

2. Experimental procedures

2.1. Material processing

AMX602 coarse powder was prepared via SWAP, as shown schematically in Fig. 1. The entire process is performed in an inert atmosphere. The molten AMX602 is directly streamed into the chamber where water is spun around the interior surface. Impinging water droplets rapidly cool the molten stream, which locks in a fine-grained microstructure. The powder is consolidated into a green compact and extruded into the final shape. The bar geometry investigated here is the same as the initial batch produced previously [26,27,30], with a compaction and extrusion temperature of 250 °C. For the plate geometry, the powder was consolidated and extruded at 370 °C into a cross section of 152 mm × 25.4 mm (6:1 width-to-thickness ratio). There is some oxidation of the molten Mg when it interacts with the water, according to Kondoh et al. [25], however the concentration was not quantified. We scanned an approximately 100 × 100 μm^2 area of the plate geometry using energy dispersive x-ray spectroscopy (EDS) and measured an oxygen concentration of 0.8 wt%. The oxygen EDS map (not shown) indicated a generally uniform distribution over the area scanned, which is consistent with [25]. In this paper, AMX602 refers to the final extruded material. The response of the compact and extruded powder were not considered in this work, but was done by previous authors [25,27,29].

2.2. Electron backscatter diffraction analysis

A FEI Nova NanoSEM 600 SEM (FEI Co. Hillsboro, OR, USA) was used to characterize the microstructure of AMX602. Electron backscatter diffraction (EBSD) characterization was used to quantify crystallographic orientations in the samples at a 20 kV accelerating voltage and at 70° tilt with an EDAX EBSD system (EDAX Inc. Mahwah, NJ) in the SEM. EBSD patterns were collected with a step size of 0.2 μm on the ED-TD plane in the middle of the plate, and approximately in the middle of the plate thickness (i.e. middle of the normal direction of the plate). The collected data was minimally "cleaned" by using the TSL OIM Analysis 7 "cleanup"

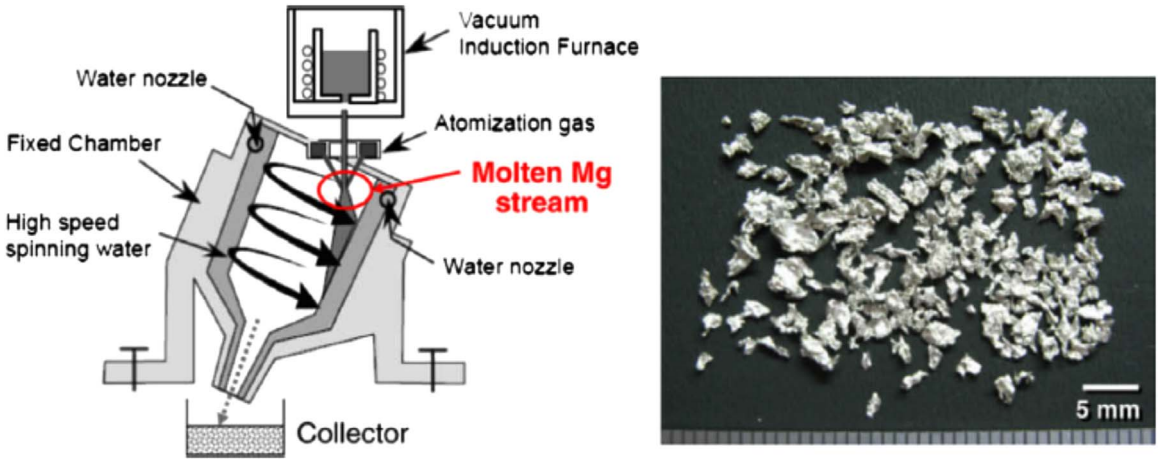

Fig. 1. Schematic of SWAP equipment to produce AMX602 powder (left) and morphology of the powder [25].

program to correct inaccurately indexed points based on neighboring point's orientation correlation. A minimum of 150,000 grains are used to quantify the texture.

2.3. Quasi-static and dynamic compression experiments

Samples cut from the bar and plate were loaded to failure in compression at quasi-static and dynamic loading rates along the extrusion (ED), transverse (TD) and normal directions (ND). Quasi-static compression experiments were performed using a screw-driven Instron machine at a constant displacement rate corresponding to a nominal strain rate of $10^{-4}\,s^{-1}$. Two strain gages mounted on orthogonal surfaces measured strain on the specimens, which were 8.5 mm × 8.5 mm × 12.7 mm. Dynamic compression experiments were performed on 11.4 and 6.35 mm cubic samples for the plate and bar geometries, respectively, using a split-Hopkinson pressure bar (SHPB) with 19 mm diameter maraging steel bars. The stress-strain history of the sample was calculated from the incident, reflected and transmitted strain gage signals mounted on the incident and transmitted bars [32]. The nominal strain rate was approximately $1000\,s^{-1}$. All samples were cut from the center of the plate and bar to eliminate any surface effects.

3. Modeling framework

We used a combined crystal- and macro-plasticity framework to model the quasi-static and dynamic response of AMX602 specimens. Elsewhere Becker and Lloyd [31] describe details of the model, so herein we restrict ourselves to essential model features and assumptions.

The model uses a pseudo-slip description for extension twinning that neglects twin reorientation effects on the mechanical response, and assumes slip-based mechanisms are basal ⟨a⟩ slip, prismatic ⟨a⟩ slip, and pyramidal ⟨c+a⟩ slip. Following Graff et al. [33] the inelastic velocity gradient is partitioned according to the individual mechanisms, i.e.,

$$\mathbf{L}^P = \sum_{\alpha=1}^{6} \dot{\gamma}^{\alpha}_{\text{twin}}\left(\mathbf{s}^{\alpha}_{\text{twin}} \otimes \mathbf{m}^{\alpha}_{\text{twin}}\right) + \sum_{\alpha=1}^{3} \dot{\gamma}^{\alpha}_{\text{bas}}\left(\mathbf{s}^{\alpha}_{\text{bas}} \otimes \mathbf{m}^{\alpha}_{\text{bas}}\right) + \sum_{\alpha=1}^{3} \dot{\gamma}^{\alpha}_{\text{pris}}\left(\mathbf{s}^{\alpha}_{\text{pris}} \otimes \mathbf{m}^{\alpha}_{\text{pris}}\right) + \sum_{\alpha=1}^{6} \dot{\gamma}^{\alpha}_{\text{pyrm}}\left(\mathbf{s}^{\alpha}_{\text{pyrm}} \otimes \mathbf{m}^{\alpha}_{\text{pyrm}}\right),$$

where, for example, $\mathbf{s}^{\alpha}_{\text{twin}}$ and $\mathbf{m}^{\alpha}_{\text{twin}}$ denote the deformation plane direction and normal of twin system α, respectively. The reduced-order model is based on simplifications of the above relations for computational efficiency and stability, so that the framework can be used to simulate large dynamic problems of interest. The model approximates the combined effect of basal ⟨a⟩ slip by assuming basal slip occurs on one aggregate system in the direction of maximum shear stress on the basal plane, denoted $\hat{\mathbf{s}}_{\text{bas}}$, such that

$$\sum_{\alpha=1}^{3} \dot{\gamma}^{\alpha}_{\text{bas}}\left(\mathbf{s}^{\alpha}_{\text{bas}} \otimes \mathbf{m}^{\alpha}_{\text{bas}}\right) \rightarrow \dot{\gamma}_{\text{bas}}\left(\hat{\mathbf{s}}_{\text{bas}} \otimes \mathbf{m}_{\text{bas}}\right),$$

where the basal slip normal is identical for all 3 systems. Because prismatic and pyramidal have similar strengths, and their combined effect forms an approximately closed yield surface in biaxial stress space [34], they are approximated using as a single isotropic, rate-dependent plastic deformation mechanism, i.e.,

$$\sum_{\alpha=1}^{3} \dot{\gamma}^{\alpha}_{\text{pris}}\left(\mathbf{s}^{\alpha}_{\text{pris}} \otimes \mathbf{m}^{\alpha}_{\text{pris}}\right) + \sum_{\alpha=1}^{6} \dot{\gamma}^{\alpha}_{\text{pyrm}}\left(\mathbf{s}^{\alpha}_{\text{pyrm}} \otimes \mathbf{m}^{\alpha}_{\text{pyrm}}\right) \rightarrow \dot{\epsilon}_{\text{slip}} \frac{3\boldsymbol{\sigma}'}{2\sigma_{vm}},$$

where $\dot{\epsilon}_{\text{slip}}$ denotes the equivalent plastic slip rate, $\boldsymbol{\sigma}'$ denotes the deviatoric portion of the Cauchy stress, and σ_{vm} is the von Mises equivalent stress. Following these approximations, the plastic velocity gradient for the reduced-order model is expressed as

$$\mathbf{L}^P = \sum_{\alpha=1}^{6} \dot{\gamma}^{\alpha}_{\text{twin}}\left(\mathbf{s}^{\alpha}_{\text{twin}} \otimes \mathbf{m}^{\alpha}_{\text{twin}}\right) + \dot{\gamma}_{\text{bas}}\left(\hat{\mathbf{s}}_{\text{bas}} \otimes \mathbf{m}_{\text{bas}}\right) + \dot{\epsilon}_{\text{slip}} \frac{3\boldsymbol{\sigma}'}{2\sigma_{vm}}.$$

Despite the seemingly restrictive set of kinematic assumptions employed in the reduced-order model, it has been shown to reliably capture the mechanical response of single-crystal Mg [31,35].

Differing constitutive relations and material parameters are used to describe the disparate responses of the three deformation mechanisms. Basal slip is assumed to be rate-independent, and its flow stress evolves according to a Voce-type hardening law [36], where

$$\tau_{bas} = \tau_{0,\text{bas}} + \tau^{\infty}_{\text{bas}}\left[1 - \exp\left(\frac{-h_{\text{bas}}\gamma_{\text{bas}}}{\tau^{\infty}_{\text{bas}}}\right)\right].$$

Extension twinning is also assumed to be rate-independent, and the flow stress on each twin system evolves as

$$\tau^{\alpha}_{\text{twin}} = \tau_{0,\text{twin}} + h_{\text{twin}}\gamma^{\text{tot}}_{\text{twin}},$$

where $\gamma^{\text{tot}}_{\text{twin}} = \sum_{\alpha=1}^{6}\gamma^{\alpha}_{\text{twin}}$, and $\tau^{\alpha}_{\text{twin}}=\infty$ when $\gamma^{\text{tot}}_{\text{twin}}\geq 0.1289$. This model assumes twin resistance increases linearly and proportionally to the total amount of twinning that has occurred on all twin systems, which is equivalent to assuming isotropic cross hardening. The resistance of prismatic and pyramidal slip is assumed to be rate-dependent, and influenced by the extent of basal slip and twinning, such that

$$\sigma_{\text{slip}} = \left\{\sigma_{0,\text{slip}} + \sigma^{\infty}_{\text{slip}}\left[1-\exp\left(\frac{-h_{\text{slip}}(\epsilon_{\text{slip}} + q_{\text{bas}}\gamma_{\text{bas}})}{\sigma^{\infty}_{\text{slip}}}\right)\right] + g_{\text{slip}}\left(q_{\text{bas}}\gamma_{\text{bas}} + q_{\text{twin}}\gamma^{\text{tot}}_{\text{twin}}\right)\right\}\left(\frac{\dot{\epsilon}_{\text{slip}}}{\dot{\epsilon}_0}\right)^{m}.$$

In the above equation g_{slip} is a linear hardening term that causes basal slip and twinning to cross-harden the combined prismatic and pyramidal slip systems, where q_{bas} and q_{twin} control the rate of cross hardening. Note that basal slip is assumed to also affect the rate that slip approaches its saturation stress in the Voce-type relation, i.e., $\sigma_{0,\text{slip}} + \sigma^{\infty}_{\text{slip}}$. Material parameters for the constitutive model are given in Table 1.

Table 1
Material parameters for reduced-order crystal model of AMX602.

Parameter	Value	Units
$\tau_{0,\text{bas}}$	80	MPa
$\tau^{\infty}_{\text{bas}}$	10	MPa
h_{bas}	$5*10^3$	MPa
$\tau_{0,\text{twin}}$	80	MPa
h_{twin}	50	MPa
$\sigma_{0,\text{slip}}$	160	MPa
$\sigma^{\infty}_{\text{slip}}$	250	MPa
h_{slip}	10^4	MPa
g_{slip}	125	MPa
q_{bas}	2	–
q_{twin}	15	–
$\dot{\epsilon}_0$	1	s^{-1}
m	0.01	–

4. Results and discussion

4.1. As-received AMX602 microstructures

Fig. 2 shows the microstructure of the AMX602 plate specimen revealed using EBSD. The scan shows nearly equiaxed grains with diameters ranging from 0.5 to 5 μm. Elongated grains larger than 10 μm in size were sparsely distributed throughout in other scans (not shown). During SWAP, the rapid cooling of the molten material likely created the elongated grains, which solidified slower than the surrounding region allowing those particular grains to grow larger. Additionally, no obvious porosity is observed. The bar geometry microstructure is characterized elsewhere [26]. It has a slightly finer grain size when extruded at 300 °C and a much larger grain size when extruded at 400 °C.

We sampled random orientations from the EBSD maps obtained in this work for the plate, and in prior work for the bar geometry [26], and these orientations are projected onto the experimental $\{0002\}$ and $\{10\bar{1}0\}$ pole figures (Fig. 3). Note the gray-scale shading is the same for all the pole figures but the scale values are different for each. In the plate (Fig. 3(a)), the basal texture is orientated primarily in the ND, which is consistent with a rolled HCP material, albeit with a much weaker peak intensity. The prismatic planes are preferentially oriented toward the ED-TD plane and are axisymmetric about the ND. The basal texture of the bar (Fig. 3(b)) is essentially axisymmetric with respect to the ED and is distributed evenly along the TD-ND plane. This is typical extrusion texture for HCP metals. The prismatic planes are randomly orientated with a slight concentration near the ED. The plate has slightly greater basal texture than the bar (4.2 versus 2.9, respectively). The difference in the textures between plate and bar specimens is a consequence of the extrusion parameters. The initial compact for the plate was 280 mm in diameter and was subsequently extruded into a plate with dimensions of 152 mm × 25.4 mm, which is a reduction during extrusion processing in the TD of 1.8:1 and 11:1 in the ND. The plate is dominated by the reduction in thickness so the texture resembles that of a rolled plate. In contrast, the compact for the bar was reduced by a similar magnitude in both the thickness and width directions, which is similar to rod extrusion texture. This implies there will be a greater volume of material with a rolled texture as the width-to-thickness ratio is increased of the extruded geometry. Understanding how the processing history influences the overall texture, and therefore the material response, is essential for designing larger plates used in engineering-scale applications.

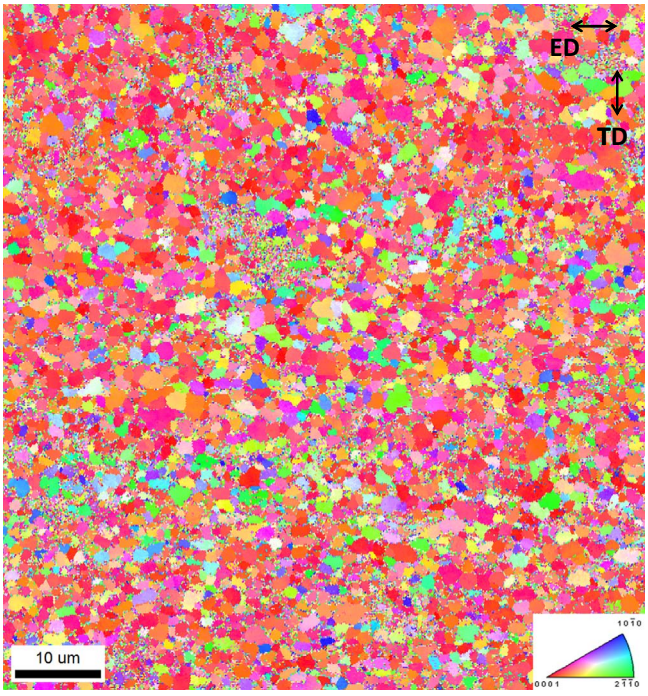

Fig. 2. EBSD map of the AMX602 plate specimen.

4.2. Mechanical behavior of AMX602

We performed compression experiments in the plate and bar at $10^{-4}\,s^{-1}$ and $1000\,s^{-1}$ in the ED, TD and ND to determine the influence of loading rate on the anisotropy of the mechanical response. All experiments resulted in the macroscopic failure of the sample, which is reflected in the stress-strain curves as a quick or sudden drop in the flow stress at large strains. Multiple experiments were performed for each geometry, loading direction, and strain rate and showed consistent results, thus, a single representative test is shown for clarity.

Fig. 4 shows the true stress-strain response for the three loading directions of the plate at quasi-static and dynamic strain rates. This figure also shows the model simulations but these results will be discussed in the next section. Compression along the ED results in a characteristic s-shaped hardening curve, which is indicative of $\{10\bar{1}2\}$ extension twinning [37]. For both strain rates, after yielding the material exhibits a nearly perfectly plastic stress plateau until strains of approximately 4%. Additionally, despite seven orders of magnitude difference in the strain rate, there is no difference in the yield strength (~280 MPa) and little difference in the post-yield stress-strain response. The dynamic strain rate has a strain to failure that is 0.04 more than for the quasi-static strain rate. Compression along the TD, Fig. 4(b), exhibits a plateau region that is less pronounced with slight hardening, and little appreciable difference in the yield strength (~240 MPa) between high and low strain rates. The subsequent work hardening rate is slightly reduced at the quasi-static strain rate and further reduced as compared to the ED. Therefore, although the strains to failure are similar for compression along the ED and TD, the peak stress at failure is lower along the TD than the ED. Fig. 4(c) shows the stress-strain response when the plate is compressed along the ND. The main differences between the response along the ND and the other two directions are the lack of a well-defined yield, a concave-down, instead of an s-shaped hardening curve, and greater strain rate sensitivity in both the initial yield strength and subsequent hardening behavior. But the work hardening rates are similar to the TD behavior. The yield strengths for quasi-static and dynamic strain rates are approximately 250 and 280 MPa, respectively.

The quasi-static and dynamic mechanical behavior of the bar geometry is shown in Fig. 5. As in the previous figure, the model simulations are plotted but will be discussed in the next section. The mechanical behavior in the ED has the same nominal s-shaped curve as the plate, with a yield strength of approximately 340 MPa and a perfectly plastic stress plateau until about 5.5% true strain. The difference in the work hardening rate between the strain rates is more pronounced in the bar as compared to the plate. Additionally, the strain-to-failure is higher in the quasi-static strain rate versus the dynamic rate. Loading in the TD (Fig. 5(b)) results in a plateau that is barely perceptible, but the yield strength is still the same between the strain rates (300 MPa). The work hardening is less for the TD of the bar than for the plate. Finally, the behavior of the bar in the ND, Fig. 5(c), shows a more pronounced plateau region than for the bar TD loading direction; this curve most resembles the TD of the plate. Both strain rates have the same yield point (290 MPa) and show a perfectly plastic flow response until

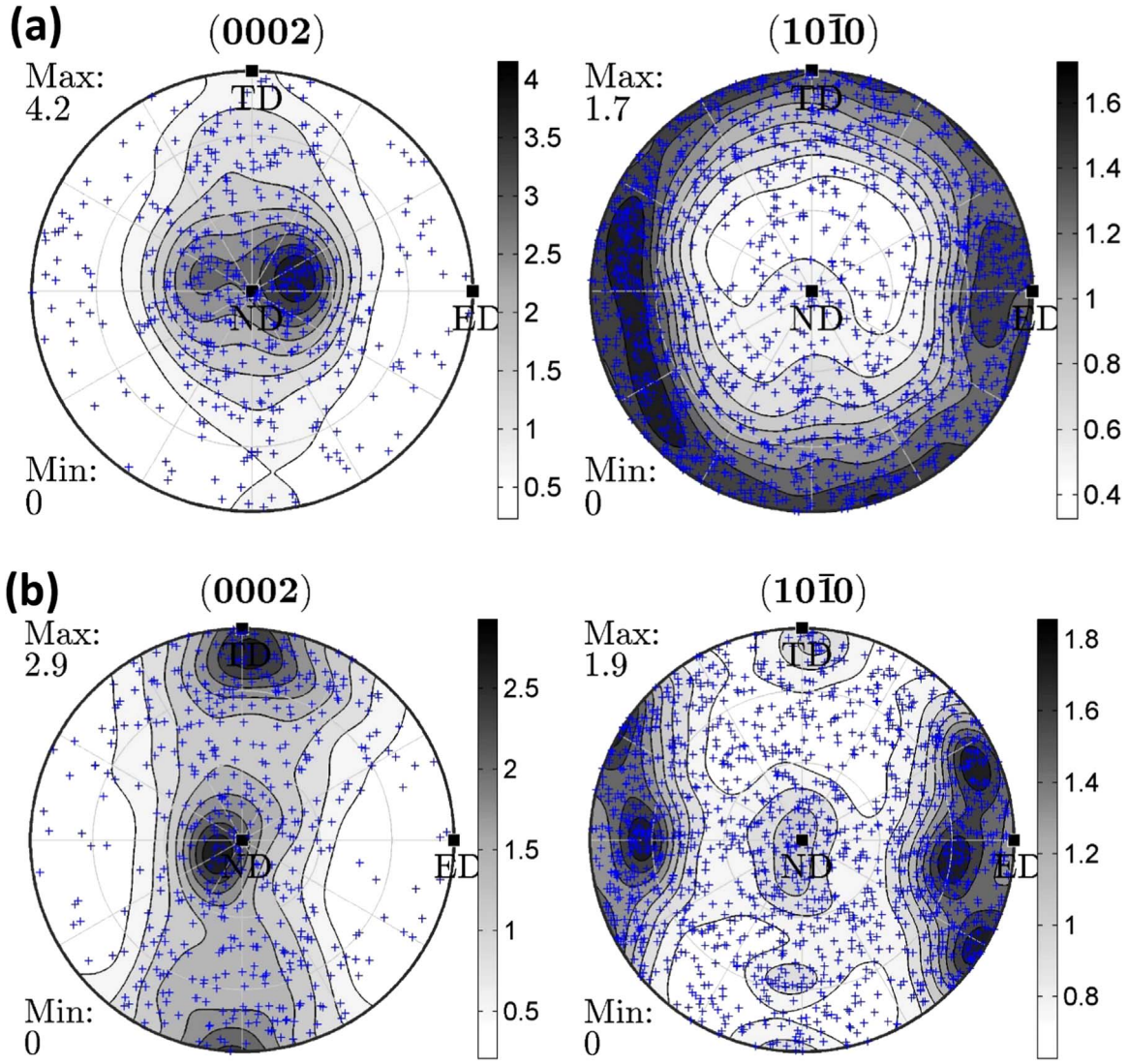

Fig. 3. Pole figures with randomly sampled orientations of AMX602 from the (a) plate and (b) bar used as input for the reduced-order HCP crystal plasticity model.

approximately 3.5% true strain. The ensuing work hardening and the dependence on the strain rate are very similar to the TD of the bar. The strain-to-failure continues the same trend with a higher value at the quasi-static strain rate.

We want to highlight three overall trends. First, the difference in the yield strengths along the three directions for each geometry are relatively low compared with conventionally processed, as well as ECAPed Mg alloys, despite sample directions coinciding with peak texture components. Two possible explanations for the reduced anisotropy are that a weak texture is formed during processing, and that the processing produces a relatively small grain size. Although the preferential textures can be used to rationalize the difference in responses along the three directions, the reduction in intensity compared with conventionally processed Mg alloys implies the difference in responses should be reduced. Additionally, several authors [8,9] have postulated that Hall-Petch strengthening is greater for twinning than for slip-based mechanisms. Therefore, as grain size is reduced, so is the relative difference in strengths between extension twinning and slip-based mechanisms.

The second trend is between the geometries: the yield strength and ductility at the quasi-static strain rates are greater in the bar than the plate samples. The former is because the extrusion temperature of the bar was lower (250° versus 370° C), which locks in the material at a higher energy state or dislocation content because it allows less recovery of the microstructure. The latter may be caused by greater porosity or powder that was not fully sintered when the plate was manufactured, as the larger dimensions permit larger temperature and stress gradients to arise. Additionally, the extrusion pressure and extrusion ratio (ratio of initial billet cross-sectional area to final cross-sectional area following extrusion) were important parameters that were different.

The final trend is there is good agreement between the bar geometry here and the results of Shen et al. [30] and Elsayed et al. [27] (the bars are from the same batch). The quasi-static behavior is similar; their results labeled “transverse direction” more closely matches our ND behavior. But they meant “transverse” as in transverse to the ED, which is true for both the TD and ND. Their yield strengths at the dynamic loading rate were greater than the quasi-static rate, while our data shows no difference. An obvious reason is their strain rate was 4000 s^{-1} versus 1000 s^{-1} in this study. We discuss the implications of the different strain rates in more detail in Section 4.4.

4.3. Model predictions of AMX602

Simulations were carried out on a cylindrical specimen with a height to diameter ratio of 1:2 to prevent any buckling effects. The

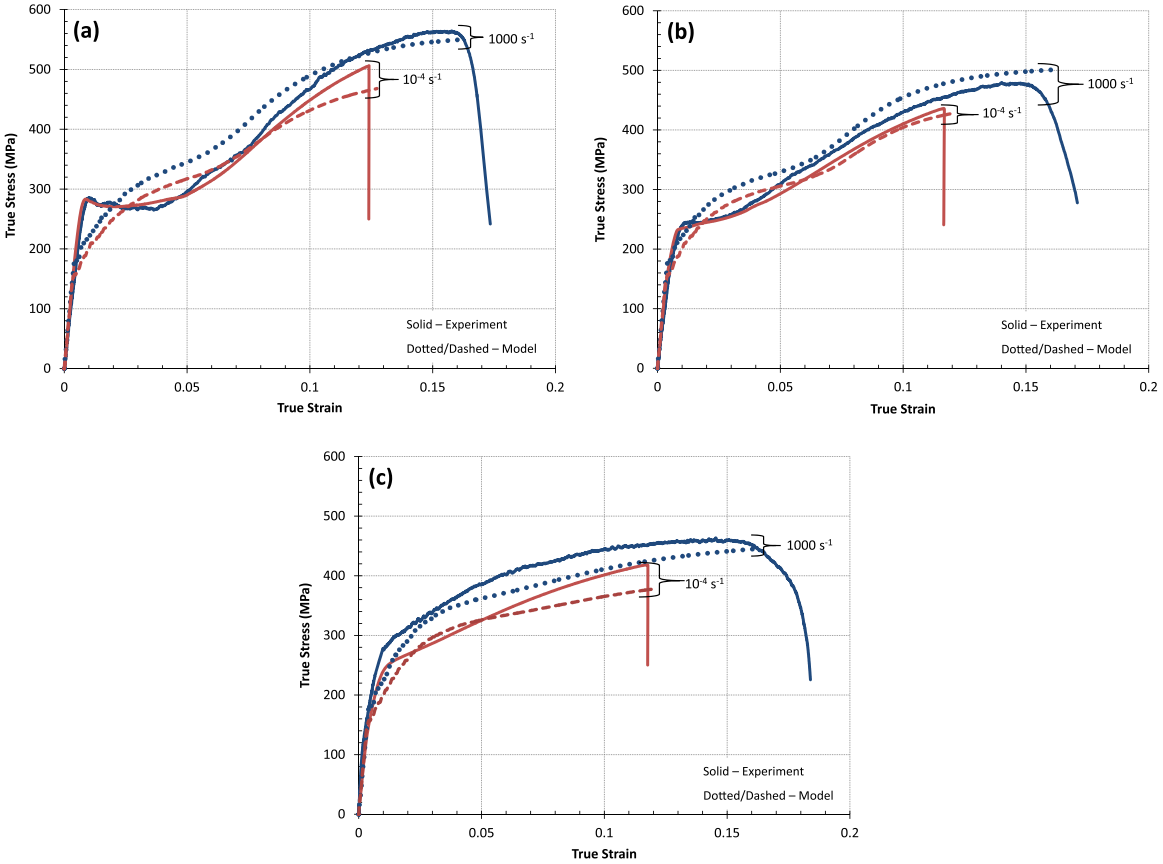

Fig. 4. Mechanical behavior and modeling of AMX602 plate in the (a) ED, (b) TD and (c) ND.

cylinder was discretized using approximately 1400 elements and contained approximately 300 grains. Increased mesh refinement and number of grains was found to have little effect of the simulated macroscopic mechanical response. Representative polycrystalline microstructures were instantiated via Voronoi tessellation with grain orientations randomly sampled from the experimentally measured pole figures. The nominal strain rate during simulations was identical to those provided experimentally. Strain to failure is not captured in the simulations as the post-bifurcation, strain localization behavior is not explicitly modeled in this work. Figs. 4 and 5 give the simulated macroscopic mechanical response of the polycrystalline aggregates that represent the AMX602 plate and bar geometries subjected to quasi-static and dynamic compressive strain rates. There are several noticeable similarities and differences between the simulated and measured responses that require further discussion.

The most pronounced difference is that the model is unable to capture the abrupt yield point, particularly when the material is thought to yield via extension twinning. The model is unable to capture such an abrupt yield point because extension twinning and basal slip alone cannot satisfy the von Mises compatibility criterion required to accommodate arbitrary deformation and cause macroscopic yielding; however, clearly the material is able to yield. Two possibilities for these differences are inherent in model approximations, most of which are common to other crystal models of HCP metals found in literature. First, the model assumes slip confined to their respective glide planes. If dislocations were allowed to cross slip or form glissile partials that act as dislocation sources on intersecting slip systems, glide on a single system would produce multiple independent deformation modes and cause yielding with fewer slip systems. Second, the model assumes that deformation due to twinning can be approximated in a "pseudo-slip" framework that smears out coordination between finite twinned domains. In reality twins appear to form coordinated patterns that demarcate finite domains of twinned and untwinned material. Direct treatment of coordinated deformation via sequential lamination has been shown to provide additional deformation modes and energy relaxation as compared to the averaged response [38,39]. As a practical substitute to soften the material response, and therefore capture the abrupt yield behavior and subsequent plateau when the material deforms via extension twinning, some authors [40,41] have employed various relaxed-constraints methods [42,43] with relative success. Although such methods are able to reproduce initial yield behavior while employing the aforementioned restrictive kinematic approximations, they act as a substitute to the rich, complex kinematics exhibited by real materials, and do not solve our deficiency in addressing them via existing continuum crystal descriptions. Therefore, we choose to use the more accurate kinematic description, i.e., direct numerical simulation of polycrystalline aggregates.

Another difference is that for yield behavior, the model does not predict a significant difference in the yield magnitudes between the plate and bar geometries, whereas the bar generally has higher initial strength in each direction. The model parameters were fit to the plate response, and no difference in processing was included when identifying material parameters. The model is only simulating the difference in the textures between the two geometries, but due to differences in the processing parameters between them, non-textural effects are manifested in the experiments. One difference is the extrusion temperature for the bar was 120 °C lower than the plate, resulting in a grain size which is 1–2 μm smaller, which would increase the yield strength. The temperature may also modify the properties of the precipitates and dislocation structures within the material, which this model does not capture.

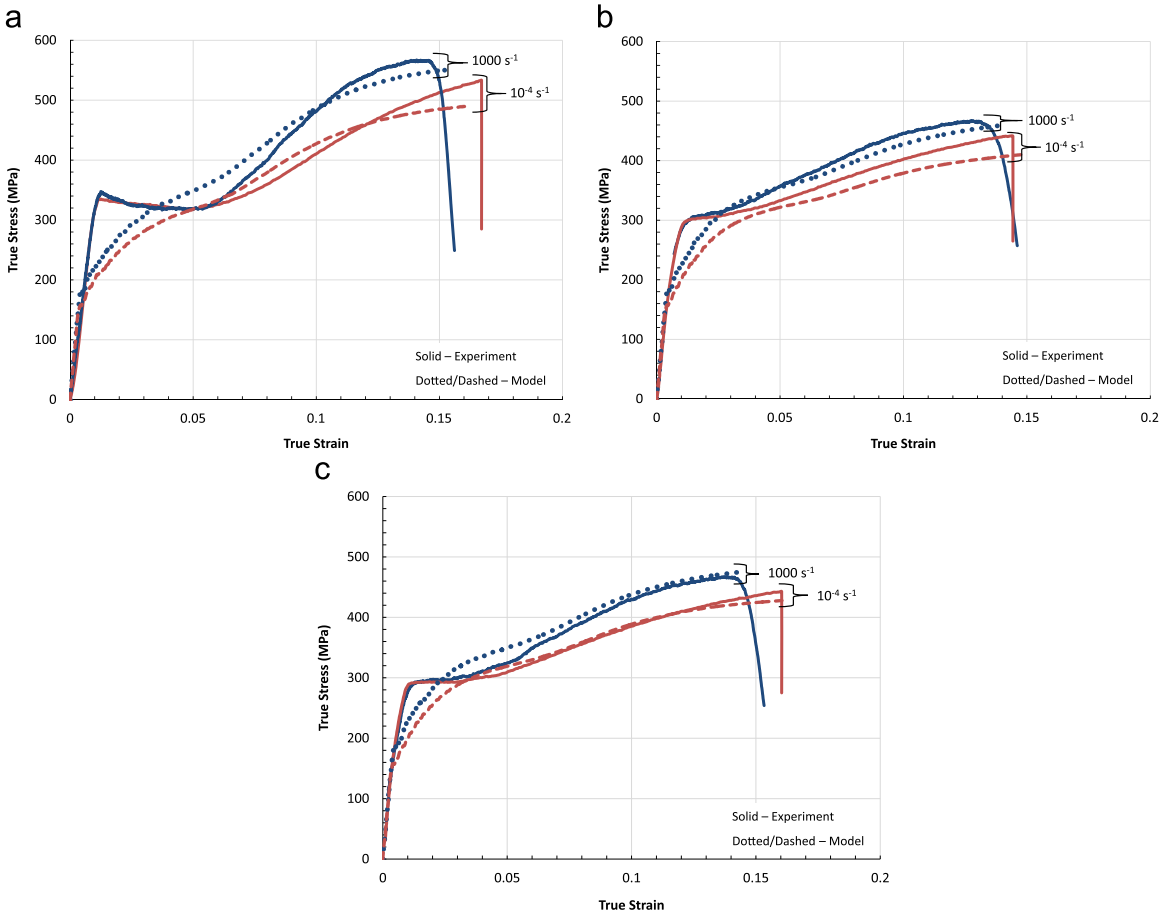

Fig. 5. Mechanical behavior and modeling of AMX602 bar in the (a) ED, (b) TD and (c) ND.

Unlike initial yield, the work hardening behavior is captured well by the model. The work hardening rate in the ED increases and is high following the plateau in the flow stress between strains of approximately 5–10%. It then decreases (but is still positive) above about 11% until failure of the specimen. Absolute differences of the hardening between the experiments and simulations could be due to the inability to reproduce the initial plateau region. The model is very successful at capturing the experimental hardening in the TD of the bar and plate and in the ND of the bar. Even the differences in the stress values are small. The deviations are larger when loading in the ND of the plate where the curves are more typical concave-down in shape, i.e. slip dominated mechanisms. Finally, the model captures well the essential differences in the mechanical behavior due to the texture difference between the plate and bar. In the TD, the model captures well the minimal plateau in the bar and a more pronounced one in the plate. This is similarly true for the ND but the plate lacks a plateau region while the bar has one.

With reasonable agreement between the predicted and measured mechanical response of AMX602, particularly in the post-yield regime, the model can provide further insight into the underlying mechanisms during plastic deformation. Fig. 6 plots the relative activity of each mechanism for the different loading conditions in the plate and bar. Fig. 6(a), (b) and (c) corresponds to loading in the ED, TD and ND, respectively. The abrupt onset of twinning causes the sudden yielding observed in Figs. 4(a) and 5 (a); however, the twinning contribution quickly reaches a maximum after a few percent true strain. Here, the mechanical response exhibits an inflection point as twinning exhausts and can no longer accommodate the applied deformation, giving way to slip. Additionally, the model and texture are able to explain why the inflection point in the work hardening in the TD occurs at a lower plastic strain than in the ED. The model indicates that the contribution of twinning is greater in the ED, and the texture is the underlying reason. Twinning is greater when loading in the ED because a greater number of basal planes are perpendicular to the ED than the TD. Twinning accommodates the c-axis extension when the material is compressed perpendicular to the c-axis. Extension twinning contributes relatively little to the overall deformation when the material is compressed along the ND (Fig. 6 (c)). Extension twin activity is suppressed, since for the idealized texture, the c-axis undergoes compression. In this case deformation is primarily accommodated by slip mechanisms, which produce a conventional parabolic, instead of s-shaped hardening curve.

In each loading direction the plate (rolling texture) versus bar (extrusion texture) geometries results in distinct effects on the deformation mechanics. The model predicts that non-basal slip is the dominant mechanism in the ED at the onset of plasticity (i.e. at yield), however, due to its high initial hardening rate it gives way to basal slip and twinning. The texture difference is predicted to have only a small effect when the material is compressed along the ED (Fig. 6(a)) because for both cases the applied load is perpendicular to the c-axis, which is consistent with the data. The strain rate is predicted to have a greater effect, but this is not observed in the data. Where the non-basal slip is greater (bar), the model predicts greater flow stress differences due to the strain rate sensitivity of these mechanisms, which matches the data. When specimens are compressed along the TD, the model predicts large differences in the amount of twinning between the plate and

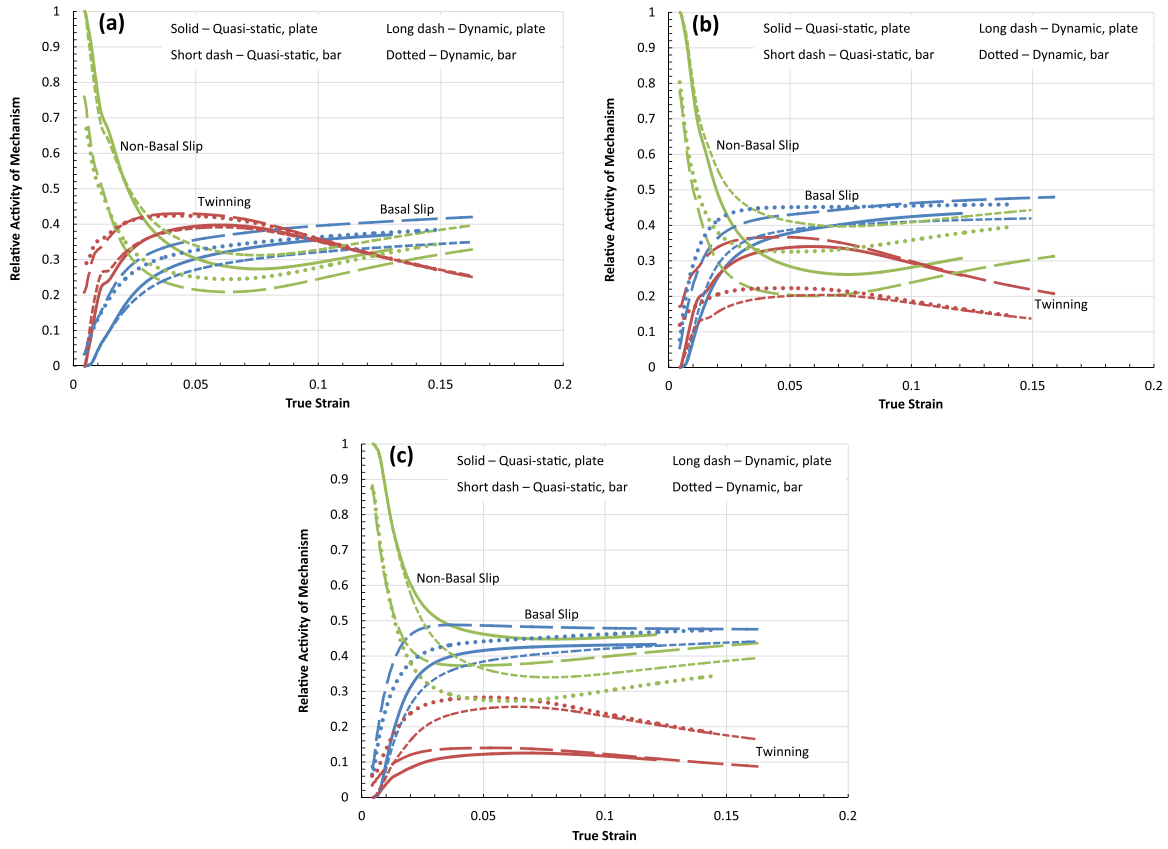

Fig. 6. Relative activity of deformation mechanisms in the (a) ED, (b) TD and (c) ND as predicted by the model.

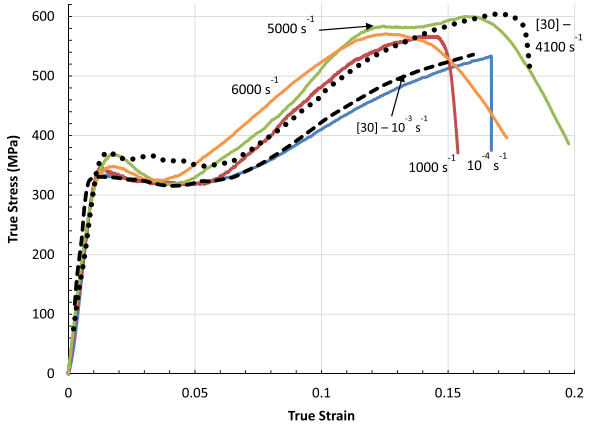

Fig. 7. Mechanical behavior of the bar in the ED showing the strain rate insensitivity of extension twinning.

bar (Fig. 6(b)). In the bar, more c-axes are orientated parallel to the loading direction than in the plate. Therefore, slip mechanisms are enhanced in the bar, causing the s-shape to become almost non-existent. Similarly, the rate-dependent non-basal mechanisms are more active in the bar than plate, resulting in the greater strain rate sensitivity observed in the bar. When plate specimens are compressed along the ND (Fig. 6(c)), the material exhibits the highest relative activity of slip, and has a typical concave down stress-strain response. Specimens taken from the bar exhibit relatively more twinning and an associated s-shaped hardening curve, similar to loading in the plate TD, where the amount of twinning is essentially the same and gives nearly an identical mechanical response. The model predicts greater strain rate sensitivity in the ND direction of the plate because the non-basal slip has the highest relative activity at true strain above several percent versus the other two directions, which is reflected in the data. Conversely for the bar, the ED data show the greatest rate sensitivity but the TD is predicted to have the highest relative activity of rate-sensitive, non-basal slip above several percent strain. Overall, the model predicts relative activity (or the trends in the activity) of the different deformation mechanisms between the geometries, loading directions, and strain rates, in a manner that is consistent with the measured mechanical responses in this study.

4.4. *Twinning strain rate sensitivity*

In all cases, except for the plate ND behavior, the quasi-static and dynamic yield points were essentially identical despite several orders of magnitude difference in the strain rate. This shows that twinning is rate insensitive over the tested strain rates, which the model assumes (the plate ND yield point is slip dominated). Shen et al. [30] shows higher yield strengths at dynamic versus quasi-static strain rates in all three loading directions for the bar. The difference is our dynamic experiments were at 1000 s^{-1} while theirs were 4100 s^{-1}. We performed higher rate experiments to see if extension twinning becomes strain rate sensitive at a threshold strain rate between 1000 s^{-1} and 4100 s^{-1}. Fig. 7 shows stress-strain curves at different strain rates in the ED of the bar and plots the corresponding data from Shen et al.. At 3200 s^{-1} (the curve is not shown for clarity) there was no indication of twinning becoming rate sensitive, where it very closely matched the 1000 s^{-1} curve. At 5000 s^{-1} there is evidence for an increase in the abrupt yield point (a 3800 s^{-1} experiment is very similar to the 5000 s^{-1} but is not shown for clarity). The yield point matches that from Shen et al. but the stress drops down to a magnitude the same as at lower strain rates (at approximately 3.5% true strain), whereas the post-yield behavior is perfectly plastic for Shen et al.. Initially we concluded this was evidence for extension twinning in

this material becoming strain rate sensitive between 3200 s^{-1} and 3800 s^{-1}.

But the observed "hump" around yielding and the subtle oscillation in the vicinity of the arrow could be wave dispersion effects between the high impedance bars and the lower impedance Mg sample, which can cause oscillations in the stress-strain curve [32]. Or error may be generated because the magnitude of the transmitted wave (which is used to calculate stress) was small relative the magnitude of the reflected wave (which is used to calculate strain and strain rate). The "hump" and subtle oscillations were present at 3800 s^{-1} also. We attempted to reduce this error by testing a sample with a reduced (loading direction) thickness. The strain and strain rate are inversely proportional to the sample thickness, so to achieve the same strain rate as a thicker sample, less input stress needs to be generated in the incident bar, i.e. the incident wave magnitude is reduced. The transmitted wave magnitude stays the same because the cross-sectional area was not changed but the reflected wave reduces in magnitude, which improves their *relative* magnitudes. A representative experiment with a reduced-thickness sample is shown at a strain rate of 6000 s^{-1} and the yield is essentially the same as at 1000 s^{-1}, i.e. no "hump", and there is no subtle oscillations in the subsequent work hardening regime of the curve. A few experiments with reduced-thickness samples at strain rates below 6000 s^{-1} are consistent with the curve shown. We should note that our data has not been filtered or smoothed in any way–the signals were only multiplied by the requisite constants to obtain stress, strain rate and strain.

Thus, our final conclusion is extension twinning for this Mg alloy is most likely not strain rate sensitive between the strains rates tested here (10^{-4} to $\sim$5000 s^{-1}), which supports the assumption of this model. The data from Shen et al. hints there could be some sensitivity, but the yield strength increase is less than 10%, so it could be variability in the behavior between samples or wave dispersion at low plastic strain producing anomalous results. It is possible twinning does become rate sensitive to a greater effect at rates beyond those tested here, but the effects of the material, grain size, texture, anisotropy, etc. on the degree of sensitivity are unknown and require further study.

5. Conclusions

In this study a high strength Mg alloy, AMX602 (Mg-6%Al-0.5% Mn-2%Ca), was produced by the spinning water atomization process (SWAP) and subsequently extruded into a plate or bar. The microstructure was fine-grained (the vast majority of grains between 0.5 and 5 μm) with relatively weak texture versus other Mg alloys. The texture differed, from an extrusion texture in the bar to a rolling texture in the plate. Quasi-static and dynamic compressive loading showed AMX602 possesses high strength, reasonable ductility and low anisotropy in the principal processing directions. Crystal plasticity modeling of the rate-dependent mechanical response was in relative agreement with the measured experimental data, especially when all the deformation mechanisms are active in abundance simultaneously. The model was used to parse the relative contribution of each deformation mechanism for given loaded cases, and study how texture differences between different extruded geometries would affect quasi-static and dynamic macroscale behavior. In the plate, the model indicated extension twinning was profuse for compression along the ED and TD, whereas slip dominated the response for compression along the ND. The mechanisms of the bar are similar to the plate, but in the ND it twins enough to have the same behavior as the TD. Finally, we see little to no evidence for extension twinning becoming strain rate sensitive over the range of strain rates tested here, which supports our model assumption.

Acknowledgements

Thanks to Tyrone Jones (ARL) for providing the material used in this investigation, Jim Catalano (ARL) for polishing samples, and David Gray (ARL) for helping with the quasi-static tests. Thanks to Rich Becker (ARL) for reviewing the manuscript.

References

[1] B.L. Mordike, T. Ebert, Magnesium properties–applications–potential, Mater. Sci. Eng. A 302 (2001) 37–45.
[2] E. Yukutake, J. Kaneko, M. Sugamata, Anisotropy and non-uniformity in plastic behavior of AZ31 magnesium alloy plates, Mater. Trans. JIM 44 (2003) 452–457.
[3] N. Stanford, M. Barnett, The origin of "rare earth" texture development in extruded Mg-based alloys and its effect on tensile ductility, Mater. Sci. Eng. A 496 (2008) 399–408.
[4] K. Hono, C.L. Mendis, T.T. Sasaki, K. Oh-ishi, Towards the development of heat-treatable high-strength wrought Mg alloys, Scr. Mater. 63 (2010) 710–715.
[5] S.R. Agnew, Ö. Duygulu, Plastic anisotropy and the role of non-basal slip in magnesium alloy AZ31B, Int. J. Plast. 21 (6) (2005) 1161–1193.
[6] J. Bohlen, M.R. Nürnberg, J.W. Senn, D. Letzig, S.R. Agnew, The texture and anisotropy of magnesium-zinc-rare earth alloy sheets, Acta Mater. 55 (2007) 2101–2112.
[7] E. Yukutake, J. Kaneko, M. Sugamata, Anisotropy and non-uniformity in plastic behavior of AZ31 magnesium alloy plate, Mater. Trans. JIM 44 (2003) 452–457.
[8] M. Barnett, A rationale for the strong dependence of mechanical twinning on grain size, Scr. Mater. 59 (2008) 696–698.
[9] M. Barnett, Z. Keshavarz, A. Beer, D. Atwell, Influence of grain size on the compressive deformation of wrought Mg-3Al-1Zn, Acta Mater. 52 (2004) 5093–5103.
[10] Y. Chen, Q. Wang, J. Peng, C. Zhai, W. Ding, Effects of extrusion ratio on the microstructure and mechanical properties of AZ31 Mg alloy, J. Mater. Process Technol. 182 (2007) 281–285.
[11] Y. Iwahashi, J.T. Wang, Z. Horita, T.G. Langdon, Principle of equal-channel angular pressing for the processing of ultra-fine grained materials, Scr. Mater. 35 (1996) 143–146.
[12] K. Kondoh, T. Aizawa, Environmentally benign fabricating process of magnesium alloy by cyclical plastic working in solid-state, Mater. Trans. 44 (2003) 1276–1283.
[13] K. Kondoh, K. Kawabata, H. Oginuma, Mechanical Properties and Texture of Hot Extruded Magnesium Alloys via RCP Process in Using Coarse Raw Powder Magnesium Technology 2007, TMS, 2007, pp. 433–436.
[14] M. Al-Maharbi, I. Karaman, I. Beyerlein, D. Foley, K. Hartwig, L. Kecskes, S. Mauthaudhu, Microstructure, crystallographic texture, and plastic anisotropy evolution in an Mg alloy during equal channel angular extrusion processing, Mater. Sci. Eng. A 528 (2011) 7616–7627.
[15] D. Foley, M. Al-Maharbi, K. Hartwig, I. Karaman, L. Kecskes, S. Mathaudhu, Grain refinement vs. crystallographic texture: Mechanical anisotropy in a magnesium alloy, Scr. Mater. 64 (2) (2011) 193–196.
[16] V. Hammond, S. Mauthaudhu, K. Doherty, S. Walsh, L. Vargas, B. Placzankis, J. Labukas, M. Pepi, M. Trexler, B. Barnett, T. Jones, L. Kecskes, Ultrahigh-strength Magnesium Alloys for the Future Force: A final Report on the 5-year Mission Program, 2009–2013, ARL-TR-6788, 2014, pp. 1–58.
[17] M. Kusy, P. Grgac, M. Behulova, A. Vyrostkova, M. Miglierini, Morphological variants of carbides of solidification origin in the rapidly solidified powder particles of hypereutectic iron alloy, Mater. Sci. Eng. A 375–377 (2004) 599–603.
[18] J. Rawers, W. Sauer, R. German, Planar solidification of rapidly solidified powders, J. Mater. Sci. Lett. 16 (1993) 1327–1329.
[19] R.N. Wright, I.E. Anderson, Age-hardening behavior of dynamically consolidated rapidly solidified Cu–2%Zr powder, Mater. Sci. Eng. A 114 (1989) 167–172.
[20] Y. Kawamura, K. Hayashi, A. Inoue, T. Masumoto, Rapidly solidified powder metallurgy Mg97Zn1Y2 alloys with excellent tensile yield strength above 600 MPa, Mater. Trans. 42 (2001) 1172–1176.
[21] Endo I, Otsuka I, R. Okuno, A. Shintani, M. Yoshino, M. Yagi, Fe-based amorphous soft-magnetic powder produced by spinning water atomization process (SWAP), IEEE Trans. Magn. 35 (5) (1999) 3385–3387.
[22] I. Yamauchi, I. Ohnaka, S. Kawamoto, T. Fukusako, Hot extrusion of rapidly solidified Al-Si alloy powder by rotating-water-atomization process, Trans. Jpn. Inst. Met. 27 (3) (1986) 195–203.
[23] I. Ohnaka, I. Yamauchi, S. Kawamoto, T. Fukusako, Production and properties of rapidly solidified Al-4.5%Cu alloy powder by the rotating-water-atomization process, J. Mater. Sci. 20 (1985) 2148–2158.
[24] K. Matsuura, M. Kudoh, H. Kinoshita, H. Takahishi, Precipitation of Si particles in a super-rapidly solidified Al-Si hypereutectic alloy, Mater. Chem. Phys. 81

(1–2) (2005) 393–395.
[25] K. Kondoh, E.-S.A. Hamada, H. Imai, J. Umeda, T. Jones, Microstructures and mechanical responses of powder metallurgy non-conbustive magnesium extruded alloy by rapid solidification process in mass production, Mater. Des. 31 (2010) 1540–1546.
[26] A. Elsayed, K. Kondoh, H. Imai, J. Umeda, Microstructure and mechanical properties of hot extruded Mg-Al-Mn-Ca alloy produced by rapid solidification powder metallurgy, Mater. Des. 31 (2010) 2444–2453.
[27] A. Elsayed, J. Umeda, K. Kondoh, The texture and anisotropy of hot extruded magnesium alloys fabricated via rapid solidification powder metallurg, Mater. Des. 32 (2011) 4590–4597.
[28] E. Ayman, U. Junko, K. Katsuyoshi, Application of rapid solidification powder metallurgy to the fabrication of high-strength, high-ductility Mg-Al-Zn-Ca-La alloy through hot extrusion, Acta Mater. 59 (2011) 273–282.
[29] T. Jones, J. Labukas, B. Placzankis, K. Kondoh, Ballistic and Corrosion Analysis of New Military-grade Magnesium Alloys AMX602 and ZAXE1711 for Armor Applications. ARL-TR-5931, 2012, pp. 1–50.
[30] J. Shen, K. Kondoh, T. Jones, S. Mathaudhu, L. Kecskes, Q. Wei, Effect of strain rate on the mechanical properties of magnesium alloy AMX602, Mat. Sci. Eng. A 649 (2016) 338–348.
[31] R. Becker, J. Lloyd, A reduce-order crystal model for HCP metals: application to Mg, Mech. Mater. 98 (2016) 98–110.
[32] ASM Metals Handbook Volume 8: Mechanical Testing and Evaluation.
[33] S. Graff, W. Brocks, D. Steglich, Yielding of magnesium: From single crystal to polycrystalline aggregates, Int. J. Plast. 23 (2007) 1957–1978.
[34] J.T. Lloyd, R. Becker, Stress-based crystal analysis of yielding in rolled Mg AZ31B, Philos. Mag. 96 (4) (2016) 370–386.
[35] E.W. Kelley, W.F. Hosford Jr., Plane-strain compression of magnesium and magnesium alloy crystals, Trans. TMS-AIME 242 (1968) 5–13.
[36] E. Voce, The relationship between stress and strain for homogeneous deformation, J. Inst. Met. 74 (1948) 537–562.
[37] A. Jain, S.R. Agnew, Modeling the temperature dependent effect of twinning on the behavior of magnesium alloy AZ31B sheet, Mater. Sci. Eng. A 462 (2007) 29–36.
[38] J.M. Ball, R.D. James, Fine phase mixtures as minimizers of energy, Arch. Ration. Mech. Anal. 100 (1984) 13–52.
[39] M. Ortiz, A. Pandolfi, Finite-deformation irreversible cohesive elements for three-dimensional crack-propagation analysis, Numer. Methods Eng. 44 (9) (1999) 1267–1282.
[40] H. Wang, B. Raeisinia, P.D. Wu, S.R. Agnew, C.N. Tomé, Evaluation of self-consistent polycrystal plasticity models for magnesium alloy AZ31B sheet, Int. J. Solids Struct. 47 (21) (2010) 2905–2917.
[41] H. Qiao, S.R. Agnew, P.D. Wu, Modeling twinning and detwinning behavior of Mg alloy ZK60A during monotonic and cyclic loading, Int. J. Plast. 65 (2015) 61–84.
[42] R.A. Lebensohn, C.N. Tomé, A self-consistent anisotropic approach for the simulation of plastic deformation and texture development of polycrystals: application to zirconium alloys, Acta Mater. 41 (9) (1993) 2611–2624.
[43] P. Van Houtte, L. Saiyi, M. Seefeldt, L. Delannay, Deformation texture prediction: from the Taylor model to the advanced Lamel model, Int. J. Plast. 21 (2005) 589–624.

1 (PDF) DEFENSE TECHNICAL INFORMATION CTR DTIC OCA

2 (PDF) DIRECTOR US ARMY RESEARCH LAB RDRL CIO L IMAL HRA MAIL & RECORDS MGMT

1 (PDF) GOVT PRINTG OFC A MALHOTRA

29 (PDF) DIR USARL
RDRL WMP C
C MEREDITH
T BJERKE
M FERMEN-COKER
R BECKER
J BRADLEY
B FAROUK
J CLAYTON
D CASEM
J LLOYD
A TONGE
C WILLIAMS
RDRL WMP B
T WEERASOORIYA
RDRL WMP E
T JONES
RDRL WML H
B SCHUSTER
B AYDELOTTE
P JANNOTTI
RDRL WMM B
B LOVE
G GAZONAS
T WALTER
D GRAY
P MOY
RDRL WMM E
J SWAB
RDRL WMM F
M TSCHOPP
L KECSKES
J LIGDA
T SANO
B BUTLER
K DARLING
H MURDOCH

INTENTIONALLY LEFT BLANK.